

# Spatiotemporal dynamics during the transition to thermoacoustic instability: Effect of varying turbulence intensities

Nitin B George, Vishnu R Unni, Manikandan Raghunathan and RI Sujith

International Journal of Spray and Combustion Dynamics  
2018, Vol. 10(4) 337–350  
© The Author(s) 2018  
Article reuse guidelines:  
sagepub.com/journals-permissions  
DOI: 10.1177/1756827717750073  
journals.sagepub.com/home/scd



## Abstract

An experimental study on a turbulent, swirl-stabilized backward facing step combustor is conducted to understand the spatiotemporal dynamics during the transition from combustion noise to thermoacoustic instability. By using a turbulence generator, we investigate the change in the spatiotemporal dynamics during this transition for added turbulence intensities. High-speed CH\* images of the flame (representative of the field of local heat release rate fluctuations ( $\dot{q}'(x,y,t)$ )) and simultaneous unsteady pressure fluctuations ( $p'(t)$ ) are acquired for different equivalence ratios. In the study, without the turbulence generator, as the equivalence ratio is reduced from near stoichiometric values, we observe an emergence of coherence in the spatial dynamics during the occurrence of intermittency, enroute to thermoacoustic instability. As the turbulence intensity is increased using the turbulence generator, we find that there is an advanced onset of thermoacoustic instability. Spatial statistics and the instantaneous fields of  $p'(t)\dot{q}'(x,y,t)$  show that during the transition from combustion noise to thermoacoustic instability, the emergence of coherent spatial structures in the instantaneous fields of  $p'(t)\dot{q}'(x,y,t)$  for the experiments with higher turbulence intensities is advanced. However, as the equivalence ratio is reduced further, we notice that higher turbulence intensities result in the reduction of the strength of the pressure oscillations during the state of thermoacoustic instability. We find that, at these low equivalence ratios, there is a decrease in the coherence due to the dispersal of  $p'(t)\dot{q}'(x,y,t)$ , which explains the reduction in the strength of the pressure oscillations.

## Keywords

Spatiotemporal dynamics, turbulent reacting flow

Date received: 6 June 2017; accepted: 23 November 2017

## 1. Introduction

Thermoacoustic instability is a critical problem faced in practical combustors such as gas turbines and rockets, when they are operated at certain conditions. This phenomenon, caused by the interactions between the heat release rate fluctuations and the acoustic pressure oscillations, leads to large amplitude pressure oscillations inside a combustor.<sup>1</sup> Suppressing or controlling these thermoacoustic oscillations is of prime importance in propulsion and power generating systems as they cause structural failure to the mechanical components of the combustor, unwanted shutdowns of the engine and monetary losses.<sup>2</sup>

There have been a number of studies in the past that focused on the dynamics during the occurrence

of thermoacoustic instability and its characterization. The transition to thermoacoustic instability is, by itself, rich in dynamics and has been investigated in the recent years. For instance, bifurcations related to combustion dynamics have been reported in several experimental studies.<sup>3</sup> Bifurcations of self-excited ducted laminar premixed flames were studied by Kabiraj et al.,<sup>4,5</sup> who established the route to chaos through quasi-periodicity and frequency locking.

Department of Aerospace Engineering, IIT Madras, Chennai, India

### Corresponding author:

Nitin B George, IIT Madras, Chennai 600036, Tamil Nadu, India.  
Email: nitinbabunit@gmail.com



Gotoda et al.<sup>6</sup> reported that thermoacoustic systems undergo a transition from stochastic fluctuations to periodic oscillations via low-dimensional chaotic oscillations when the equivalence ratio is varied. In a laminar combustor, Kabiraj and Sujith<sup>7</sup> discovered the occurrence of intermittency in thermoacoustics. Further, in turbulent combustors that use a swirler or a bluff-body as flame holding devices, Nair and Sujith<sup>8</sup> reported the presence of intermittency during the transition from stable combustion to thermoacoustic instability. They observed that, during this state of intermittency, the unsteady pressure signals display bursts of high-amplitude periodic oscillations amidst aperiodic epochs. Pawar et al.<sup>9</sup> described the onset of thermoacoustic instability as a phenomenon of mutual synchronization between the acoustic pressure oscillations and the heat release rate fluctuations. Further, they described the transition from combustion noise to thermoacoustic instability as a transition from a state of desynchronized aperiodic oscillations to generalized synchronization via intermittent phase synchronization and phase synchronization. Unni and Sujith<sup>10</sup> observed that during the occurrence of intermittency, the flame alternates between two different patterns of oscillations. Using high-speed Mie scattering images, they found that the flame oscillates in an aperiodic manner during the epochs of low-amplitude aperiodic oscillations and the flame exhibits periodic roll up during the epochs of high-amplitude periodic oscillations. Kheirkhah et al.<sup>11</sup> studied the local phase relationships between the heat release rate fluctuations and the acoustic pressure oscillations in a gas turbine combustor. They observed the development of in-phase oscillations during increasing amplitude of oscillations and the development of out of phase oscillations during decreasing amplitude of oscillations. Additionally, Mondal et al.<sup>12</sup> showed that the transition regime from combustion noise to thermoacoustic instability exhibits chimera-like states in the spatiotemporal dynamics. They showed that these chimera-like states display regions where the local heat release rate oscillations are synchronized amidst regions of desynchronized local heat release rate oscillations.

Lieuwen<sup>13</sup> studied limit cycle oscillations in a lean premixed turbulent combustor with a conical bluff-body stabilized flame. Both supercritical and subcritical Hopf bifurcations were observed in their combustor under different operating conditions. A subcritical bifurcation was observed when the combustor was operated with low-inlet velocity and high-pressure conditions, while a supercritical bifurcation was observed when the combustor was operated with higher inlet velocity and lower mean combustor pressure. Nair and Sujith<sup>14</sup> noted that the statistical properties for the pressure oscillations measured during the transition

vary smoothly for the turbulent combustor with the bluff-body and the swirl-stabilized flames. They conjectured that the presence of turbulence in the reactive flow causes intermittency which results in the smoothness of the statistical properties.

Previous studies have investigated the effect of noise on the transition characteristics in different thermoacoustic systems. They performed such studies to investigate the effect of turbulence using noise imposed on simpler laminar systems. For instance, Waugh and Juniper<sup>15</sup> demonstrated that the additive stochastic perturbations can cause triggering from low noise amplitudes to self-sustained oscillations in a Rijke tube. Further, Jegadeesan and Sujith<sup>16</sup> experimentally investigated the noise-induced triggering of a non-premixed flame operating in a bistable region. Under the influence of noise, the system underwent a transition from a stable to an oscillatory state. However, they observed that with an increase in the amplitude of the noise introduced into the system, the mean phase difference between the pressure fluctuations and the heat release rate fluctuations increased, resulting in the reduced amplitude of the periodic oscillations. Moeck et al.<sup>17</sup> investigated the subcritical bifurcation to thermoacoustic instability in a premixed combustor. Using a nonlinear model, they observed that an increase in the noise level resulted in a narrower hysteresis region. They associated this behavior with the modification of the domains of attraction of the respective equilibrium solutions. Additionally, Bonciolini<sup>18</sup> analytically investigated and compared the dynamics of white and colored noise driven self-sustained oscillators. Noiray and Schuermans<sup>19</sup> were able to estimate deterministic quantities such as the linear growth rates from noise perturbed limit cycles using stochastic differential equations. Clavin et al.<sup>20</sup> studied turbulence induced noise effects on high frequency combustion instabilities in liquid propellant rocket motors and suggested that turbulence behaves as multiplicative noise in a thermoacoustic system.

Further, Kabiraj et al.<sup>21</sup> investigated the role of noise in the parameter space before the bistable region in a model thermoacoustic system. From the experimental results, they observed that noise induces coherence (noise-induced order) in the acoustic pressure fluctuations of the thermoacoustic system. The coherence factor increased with noise intensity and then decreased after reaching optimum values at various equivalence ratios. They also noted that the coupling between the pressure fluctuations and the unsteady heat release rate fluctuations is also affected by the external noise and the system response to noise increased, as it was brought closer to the bistable region. Similarly, Kabiraj et al.<sup>22</sup> reported that the disruption of the flame/acoustic coupling is caused by

the addition of noise leading to aperiodic behavior. Gopalakrishnan and Sujith<sup>23</sup> reported that the external noise added to a Rijke tube results in a reduction in the amplitude of the limit cycle oscillations. They also reported that the width of the hysteresis zone decreases with an increase in the noise strength and the bistable zone disappears above a threshold value of the noise strength. Further, Gopalakrishnan et al.<sup>24</sup> observed the presence of stochastic P-bifurcations in the presence of low intensity noise. However, in the presence of high intensity noise, P-bifurcations were not observed. They inferred that when the hysteresis region is suppressed in the presence of high intensity noise, it corresponds to the regime with the non-existence of P-bifurcations. These previous studies show different ways in which the characteristics of the transition zone in different thermoacoustic systems have been altered under the influence of external stochastic perturbations. On the other hand, in our study, we try to investigate the changes in the transition from combustion noise to thermoacoustic instability in a turbulent combustor by varying the turbulence intensity using a turbulence generator, in the combustion chamber.

Practical combustors used in the industry are essentially turbulent, which complicates the flow field dynamics. Further, complex flow structures have been observed in such systems. Schadow and Gutmark<sup>25</sup> observed that the development of coherent flow structures leads to periodic heat release rate. When the heat release rate oscillations are in-phase with the pressure oscillations, they observed combustion instability. Precessing vortex cores have been observed in turbulent swirl-stabilized combustors, which interact with the acoustic field, resulting in a self-excited helical mode instability.<sup>26</sup> Paschereit et al.<sup>27</sup> succeeded in designing an active control system in a swirl-stabilized combustor to suppress thermoacoustic oscillations. They reported that modulating the air flow results in the variation of the mixing process between fuel, air and the hot radicals which reduces the coherence of the vortex structures, thereby suppressing the large amplitude oscillations. In turbulent combustors, a priori, we cannot predict the effect of the inherent fluctuations on the transition to thermoacoustic instability due to the formation of such complex structures.

In our study, by increasing the strength of the inherent fluctuations in the flow field, we change the characteristics of the coupling between the reactive flow and the acoustic field. We find that an increase in the turbulence intensity of the flow field using a turbulence generator results in an advanced onset of large amplitude periodic oscillations. However, we also observe that at lower equivalence ratios, the amplitude of the pressure oscillations is reduced with an increase in the turbulence levels. Instantaneous fields of  $p'(t)q'(x, y, t)$ ,

which are representative of the instantaneous local acoustic power production show the emergence of coherence in the spatial dynamics with a reduction in the equivalence ratio. Further, we observe that on decreasing the equivalence ratio, the spatial variance of the instantaneous fields of  $p'(t)q'(x, y, t)$  increases, prompting us to infer that coherent spatial structures are formed in the field of  $p'(t)q'(x, y, t)$ . This suggests that there is a change in the spatial dynamics of the interaction between the local unsteady heat release rate and the acoustic field of the combustor duct, on varying the equivalence ratio. With increased turbulence levels, we find that there is a disruption of the coherence of the spatial structures leading to the lower amplitude of periodic oscillations at low equivalence ratios. Additionally, we also observe that the advanced onset of periodic oscillations at higher equivalence ratios with higher turbulence levels is due to the increase of the spatial coherence. The outline of this paper is as follows. A description of the experimental setup is presented next. This is followed by the analyses of the results from the experiments. Finally, we draw the important conclusions from this study.

## 2. Experimental setup

The swirl-stabilized turbulent combustor used in our study shown in Figure 1(a) is adapted from the original design of Komarek and Polifke.<sup>28</sup> It is a combustor with a backward facing step. A fixed vane swirler is used to stabilize the flame. The combustion chamber has a cross-section of  $90 \times 90 \text{ mm}^2$  and is 1100 mm long. A decoupler is attached to the end of the combustion chamber to achieve the boundary condition of an open duct ( $p' = 0$ ) and to minimize the acoustic radiation losses to the surroundings. Preceding the combustor duct, there is a plenum chamber where compressed air enters, and subsequently, there is a burner section where partial premixing of fuel and air occurs. The fuel is injected into the burner assembly 100 mm upstream of the swirler. Liquefied petroleum gas (LPG) which is approximately 60% butane and 40% propane is used as the fuel for all the experiments. In this study, we represent all the experimental results with respect to the equivalence ratio ( $\phi$ ) of the combustion mixture. The maximum uncertainty in the estimated equivalence ratio calculated from the uncertainties in the measurements from the mass flow controllers is  $\pm 0.03$  (refer Nair et al.<sup>29</sup> and Nair and Sujith<sup>14</sup> for more details).

The mass flow rates of fuel and air are measured and controlled using mass flow controllers (Alicat Scientific, MCR Series) with an uncertainty of  $\pm (0.8\% \text{ of reading} + 0.2\% \text{ of full scale})$ . The mass flow rate of the fuel is  $4.96 \times 10^{-4} \text{ kg/s}$ . This flow rate corresponds to a thermal power of 24.7 KW. The unsteady pressure

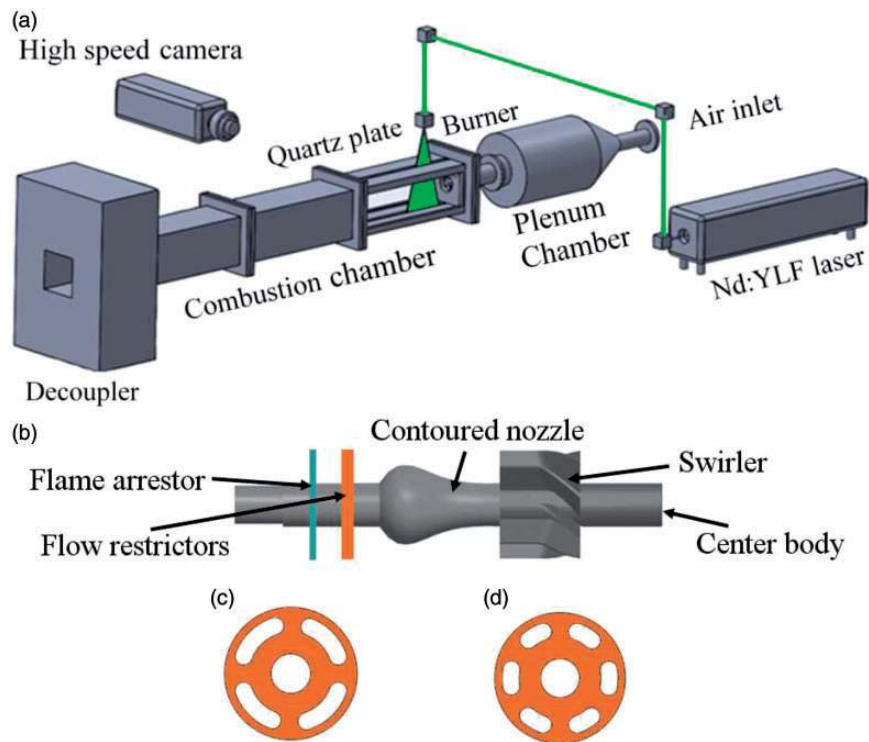


**Figure 1.** (a) The schematic of the experimental setup. (b) The burner assembly which comprised a flame arrester, followed by the turbulence generator comprising of flow restrictors and a contoured nozzle, the swirler and a center body. (c) Flow restrictor configuration corresponding to 75% blockage. (d) Flow restrictor configuration corresponding to 85% blockage.

fluctuations are measured using a piezoelectric transducer PCB103B02, which has an uncertainty of  $\pm 0.15$  Pa. The signals from the piezoelectric transducer are acquired using an A-D card (NI-6143, 16 bit) at a sampling frequency of 10 kHz. This piezoelectric transducer is not flush mounted on the combustion chamber. However, with the present mounting arrangement, there is less than  $5^\circ$  acoustic phase delay for the dominant frequency. This acoustic phase lag is not significant enough to affect the analyses described in this study. Flame images are acquired using a high-speed CMOS camera (Phantom V 12.1) operating at  $1280 \times 400$  pixels resolution with a filter (narrow band, peak at 435 nm, 10 nm FWHM) capturing the light intensity corresponding to  $\text{CH}^*$  chemiluminescence from the combustor at a sampling rate of 2 kHz. The camera is outfitted with a CARL ZEISS 50 mm camera lens at an aperture of  $f/2$ . In this manner, a  $280 \text{ mm} \times 90 \text{ mm}$  region on the combustor section is acquired on  $870 \times 280$  pixels of the sensor.

Separate particle image velocimetry experiments are performed at an optically accessible section of the duct made of quartz to acquire velocity measurements in the absence of combustion. A single cavity – double pulsed Nd:YLF laser (Photonics DM527-50) of operating wavelength 527 nm is used at a repetition rate of 4 kHz to produce the laser beam required to illuminate

the seeding particles. The laser beam is directed towards the combustion chamber using a set of right-angle prisms and a pair of convex lenses of focal lengths 500 mm and 50 mm to control its divergence. Above the turbulent combustor, the laser beam is then expanded into a laser sheet of 2 mm thickness using a 600 mm spherical lens and a  $-16$  mm cylindrical lens. The laser sheet is transmitted through a horizontal slit (5 mm width and 400 mm length) made of quartz on the top plate of the duct into the combustion chamber. Olive oil droplets with a size of approximately  $1 \mu\text{m}$  are used as the seeding particles. A Laskin nozzle is used to produce these droplets. A high-speed CMOS camera (Phantom V 12.1) operating at  $1280 \times 800$  pixels, synchronized with the laser is used to capture the Mie scattered light from the seeding particles onto single frame – single exposed images. The camera is outfitted with a CARL ZEISS 50 mm camera lens with an aperture of  $f/5.6$ . Subsequently, a  $126 \text{ mm} \times 90 \text{ mm}$  section of the combustor is imaged on  $1092 \times 780$  pixels of the camera sensor. A bandpass optical filter centered at 527 nm (10 nm FWHM) is mounted in front of the lens to capture only the Mie scattered light. The seeding particle density was large enough to achieve more than the required particles in the interrogation windows for PIV image processing. The time delay between the pulses is kept fixed at  $30 \mu\text{s}$  to achieve

a displacement of the seeding particles of approximately four pixels on the camera sensor.

The Mie scattered images are processed using PIVview software from PIVtec GmbH.<sup>30</sup> The velocity field is calculated from the Mie scattered image pairs divided into interrogation windows of  $32 \times 32$  pixels. The cross-correlation algorithm with a multi-pass approach (three passes) and least square Gaussian fit peak search scheme are chosen as the evaluation method and peak detection scheme, respectively.<sup>31</sup> A 50% overlap is chosen between the interrogation windows. Post-processing algorithms are used to detect and replace a small number of outliers. The velocity uncertainty from the PIV experiments in our study is approximately 2.5% which is calculated using the minimum subpixel displacement of 0.1 pixels<sup>31</sup> and the maximum pixel displacement of 4 pixels in the bulk flow region. This uncertainty is a result of the usage of small values of pixel displacement. However, we use small values of pixel displacement in between the laser pulses to reduce the out-of-plane movement of the seeding particles in swirling flows. The particle image sizes are approximately between two and three pixels. This corresponds to a maximum uncertainty of 0.1 pixels due to the peak locking effects.<sup>32</sup> The laser sheet is approximately 2 mm thick. On considering a maximum out-of-plane movement of 4 pixels, an uncertainty of 0.2 pixels is expected<sup>32</sup> for particle image sizes of 2.5 pixels. This would result in a relative error of 5% for the velocity measurements. Low-velocity regions in the flow field have a pixel displacement of approximately 0.2 pixels. This can account for large uncertainties in the range of 50% in these low-velocity regions.

The burner assembly shown in Figure 1(b) comprises flow restrictors located upstream of a contoured nozzle followed by the swirler and a center body. Flow restrictors create a blockage in the flow and consequently, vortices are produced. The key idea behind the design of this turbulence generator is that a vortex that impinges on the contoured nozzle disintegrates into smaller vortices through a turbulent cascade producing fine scale turbulence.<sup>33</sup> The intensity of the impinging vortex can be changed either by varying the blockage or by varying the mean flow velocity. The design of the turbulence generator shown in the figure is inspired by the studies of Videto and Santavicca<sup>34</sup> and Marshall et al.<sup>33</sup> Further details on the generation and variation of turbulence intensity using flow restrictors can be found in these articles. Using this arrangement, the turbulence intensity can be varied without changing the mean flow velocity.

Three cases are investigated in this experimental study. The first case, referred to as case A, does not contain the turbulence generator assembly and uses only the swirler in the burner housing. The second

case, referred to as case B, uses the turbulence generator with the configuration of the flow restrictor as shown in Figure 1(c). The blockage, in this case, is approximately 75%. Case C uses the turbulence generator arrangement with the flow restrictor configuration shown in Figure 1(d) and it has a blockage of approximately 85%.

### 3. Results

Typical gas turbine combustors are operated with relative turbulence intensities up to 30%.<sup>33</sup> In our study, we obtain turbulence intensities in the range of 30% to 50% in the shear layer region in the absence of the flame. However, it is critical to note that since a turbulent flame is spatially extended, the flow field, the dominant flow structures and the subsequent distribution of the turbulence intensity are also important to analyse. Nevertheless, these experiments can provide a preliminary understanding of the effect of the inherent turbulence intensity on the transition dynamics where the interactions between the flame, the hydrodynamics, and the acoustic field are highly intertwined.

There have been previous studies which have investigated the effect of turbulence by modeling it as forcing with stochastic noise. Previously, Waugh and Juniper<sup>15</sup> reported that a thermoacoustic system will dislodge itself from the oscillatory solution if the noise amplitude is sufficiently high. Lieuwen and Banaszuk<sup>35</sup> considered turbulence as noise in the base state, characterized by aperiodic oscillations. They studied the significance of parametric noise sources in exerting qualitative changes on the combustion dynamics in turbulent combustors. A priori, we cannot predict the effect of higher turbulence intensity on the transition behavior in a turbulent combustor. We try to investigate the effect of increased turbulence intensity, through the use of a turbulence generator, on the dynamics of the thermoacoustic system. Subsequently, we investigate the early onset of thermoacoustic instability and the reduction in the strength of the self-sustained periodic oscillations with higher turbulence intensities.

The time-averaged turbulence intensity fields (a, c and e) and the corresponding time-averaged vorticity fields (b, d and f) obtained from the PIV experiments are presented in Figure 2. Cold flow experiments are performed to quantify the level of turbulence in the combustor duct in the absence of thermoacoustic feedback. The air flow rates are fixed for these experiments and they correspond to the air flow rate at the equivalence ratio,  $\phi = 0.46$ , used for experiments with the flame. The  $xy$ -plane shown here corresponds to a window of  $126 \text{ mm} \times 90 \text{ mm}$  in size and the left side aligns with the dump plane of the combustion chamber. The bulk flow is thus from the left to the right.

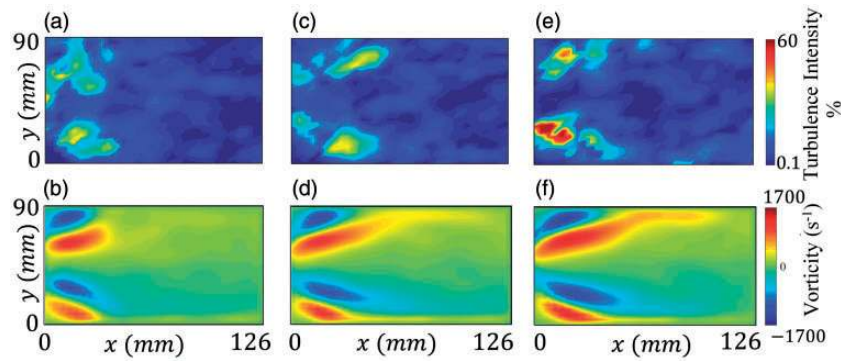


**Figure 2.** Time-averaged turbulence intensity fields and the corresponding time-averaged vorticity fields obtained from cold flow experiments for case A (a, b), case B (c, d) and case C (e, f) downstream of the dump plane, where  $x$  refers to the horizontal distance from the dump plane and  $y$  refers to the position in the vertical plane.

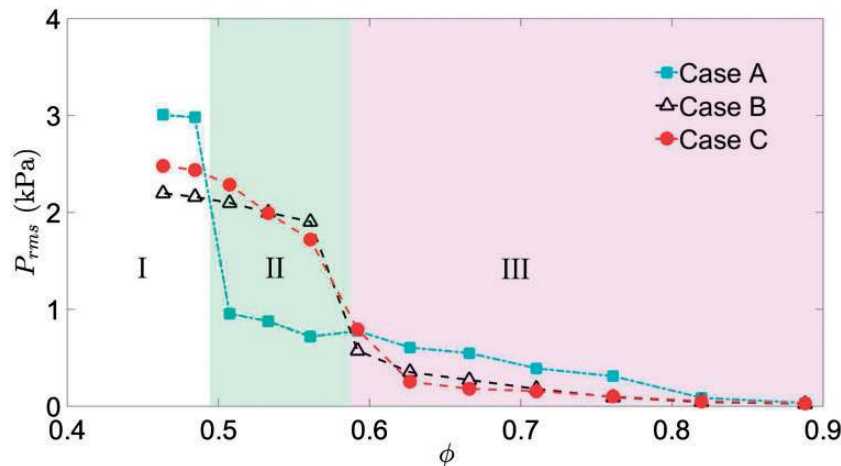


**Figure 3.** Variation of the rms of the unsteady pressure fluctuations ( $P_{rms}$ ) with respect to equivalence ratio  $\phi$  is plotted for the various cases studied. We perform the experiments starting at  $\phi = 0.89$  and vary it to 0.46 for all the experiments.

The time-averaged turbulence intensity (rms) is obtained by calculating the ratio between the velocity fluctuations ( $u'$  and  $v'$ ) and the bulk flow velocity ( $U$ ) at the burner exit (Turbulence intensity =  $\sqrt{(u'/U)^2 + (v'/U)^2}$ ). Figure 2(a) and (b) shows the time-averaged turbulence intensity field (rms) and the corresponding time-averaged vorticity field for case A, which is without the turbulence generator (flow restrictor and contoured nozzle) in the burner assembly. Figure 2(c) and (d) corresponds to the velocity measurements with case B, while Figure 2(e) and (f) refers to the velocity measurements for case C. The fields of turbulence intensity show higher intensities downstream of the dump plane in the shear layer as the blockage is increased. These experimental results are consistent with those found in the studies by Videto and Santavicca<sup>34</sup> and Marshall et al.<sup>33</sup> Higher vorticity

strength can be observed in the shear layer regions for cases B and C when compared to case A.

Combustion experiments are performed to observe the effect of the modified flow field and, in particular, the effect of higher turbulence intensities in the reactive field. The fuel flow rate is maintained constant and the air flow rate is varied. In such a manner, the equivalence ratio is varied from  $\phi = 0.89$  to  $\phi = 0.46$ , for all the experiments. For all these experiments, we are away from the regime of lean blowout. For the current setup, we expect lean blowout to occur below the equivalence ratio of 0.3 since we have a partially premixed flame. The root mean square value of the unsteady pressure fluctuations is plotted in Figure 3 as a function of the equivalence ratio for all the three cases investigated in our study. We can observe three zones in this figure.

In zone III, where the equivalence ratio is close to the stoichiometric ratio, we can observe that the root

mean square value of the pressure fluctuations ( $P_{rms}$ ) is relatively larger for case A in comparison to those for cases B and C. As the equivalence ratio is reduced, we find a region (zone II) where  $P_{rms}$  is larger for cases B and C in comparison to case A (near  $\phi = 0.6$ ). It appears that the onset of large amplitude periodic oscillations is advanced with an increase in the turbulence intensities in the reactive flow field. The time trace of these pressure oscillations in zone III and II is shown later in Figure 4. With further decrease in the equivalence ratio (zone I), we observe a reduction in the  $P_{rms}$  for the cases with higher turbulence intensities when compared to case A. There is approximately 25% (case B) decrease in the  $P_{rms}$  when compared to case A. Further, we observe that the  $P_{rms}$  corresponding to case B is marginally lesser compared to case C which represents the case with the highest blockage and hence the highest turbulence intensities. This suggests that further increase in the turbulence levels does not guarantee a larger decrease of the  $P_{rms}$ . However, a more exhaustive study, which includes simultaneous flame imaging and velocity measurements, is required to understand why the  $P_{rms}$  does not decrease further with an increase in the turbulence intensity. Nevertheless, higher turbulence intensities for the cases B and C have resulted in a smaller  $P_{rms}$  than case A.

The plot of  $P_{rms}$  with respect to the equivalence ratio indicates the change in the transition characteristics with the increase in the turbulence levels. Higher turbulence levels have resulted in a decrease of the stability margin. At the same time, the increase in the turbulence levels has not resulted in a drastic reduction of the

amplitude of the pressure oscillations at low-equivalence ratios. Nevertheless, a turbulent flame is spatially extended and the distribution of the turbulence intensity due to the presence of vortices in the flow field could have equally significant effects on the combustion dynamics during the occurrence of thermoacoustic instability. More importantly, it is critical to understand the reason behind the advanced onset of thermoacoustic instability at higher levels of turbulence by performing simultaneous imaging of the flame and PIV measurements. It is likely that large scale coherent flow structures emerge in the shear layer region earlier for the cases with higher turbulence levels, thereby causing an advanced onset of large amplitude oscillations.

Our results are similar to those obtained by Gopalakrishnan and Sujith<sup>23</sup> in a Rijke tube where they studied the effects of noise on the bistable regime. They observed that the addition of higher noise strength into a laminar system led to a reduction in the  $P_{rms}$ . In our experiments, even though the  $P_{rms}$  is reduced with the presence of flow restrictors, there is an advanced onset of large amplitude pressure oscillations due to the high turbulence levels in the reactive flow field. These results could possibly be compared to the study by Jegadeesan and Sujith.<sup>16</sup> They observed that, under the influence of random fuel flow rate fluctuations behaving as parametric noise, the thermoacoustic system transitions to an oscillatory state with excitation using noise amplitudes are significantly lower than the triggering amplitude, resulting in an advanced onset of periodic oscillations. Previous

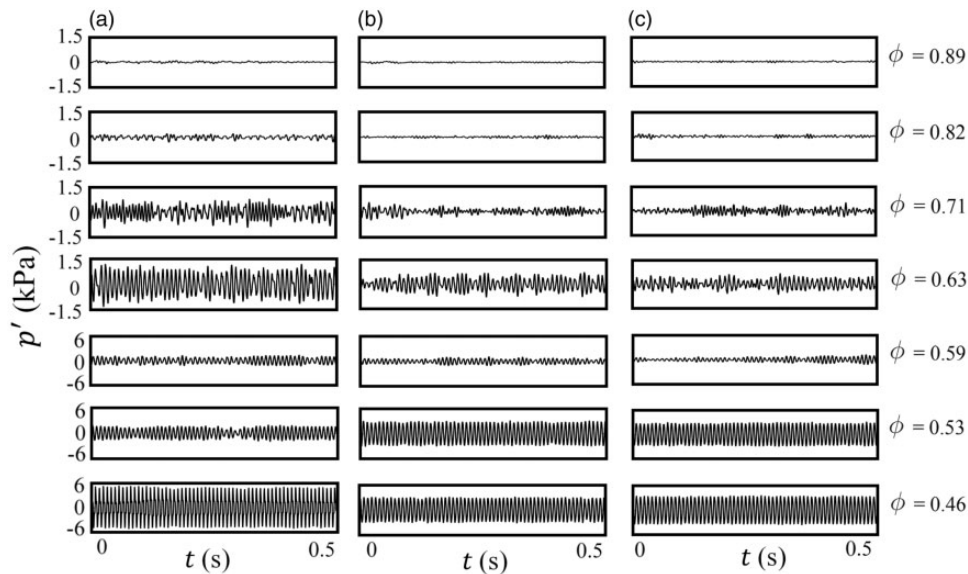


**Figure 4.** Time trace of the unsteady pressure fluctuations for case A (a), case B (b) and case C (c) at  $\phi$  varying from 0.89 to 0.46. Note the change of scale of the ordinate for  $\phi = 0.59, 0.53$  and  $0.46$ .

studies on noise-induced transitions<sup>36,37</sup> have investigated the effect of noise on the dynamics of a system. They have shown that noise can cause bifurcations and introduce new dynamical states in these systems. In our experiments, it is the higher turbulence levels in the reactive flow which have caused an advanced onset of the self-sustained periodic oscillations. Further, in our study with case A, the onset of large amplitude oscillations appears to be a sudden transition at the equivalence ratio of 0.48. In contrast, the introduction of higher turbulence intensities has resulted in a relatively more gradual onset of the large amplitude oscillations.

The unsteady pressure fluctuations are shown in Figure 4 for all the three cases for  $\phi$  varying from 0.89 to 0.46. We can perceive that the amplitude of the pressure fluctuations increases as  $\phi$  is reduced for all the three cases. Further, we also observe the occurrence of intermittency at  $\phi = 0.71$  and 0.63. Additionally, during the state of intermittency at  $\phi = 0.71$  for case A, we observe that the amplitude of the periodic oscillations is significantly higher than those of the corresponding cases of B and C. Even though the pressure oscillations at  $\phi = 0.63$  for case A resemble periodic oscillations, there are aperiodic epochs of very small duration. Further, the unsteady pressure oscillations resemble intermittent oscillations for case A up to  $\phi = 0.53$ , while those for cases B and C resemble intermittent oscillations up to  $\phi = 0.59$ . It appears that the intermittent state is observed for a wider range of equivalence ratios for the case A, which is with lower turbulence. Further, the significant rise in the value of  $P_{rms}$  (zone II) observed in Figure 3 for the cases B and C corresponds with periodic oscillations and not intermittent oscillations.

Performing fast Fourier transform (FFT) on the pressure fluctuations at  $\phi = 0.63$  provides the frequencies of the most dominant modes and their corresponding strengths. In Figure 5, we observe that the most

dominant modes are 103.5 Hz for case A (a), 108 Hz for case B (b), and 105 Hz for case C (c) at  $\phi = 0.63$ . Further, the FFT plot also shows that the amplitude spectrum value corresponding to the most dominant mode of case A is approximately 50% more than the corresponding values of cases B and C at  $\phi = 0.63$ . It is critical to note that the amplitudes of the dominant modes are relatively low at  $\phi = 0.63$  when compared to  $\phi = 0.46$ . The frequency of the pressure oscillations obtained from FFT at  $\phi = 0.46$  shows that the dominant frequency does not change much as the turbulence intensity is increased. Further, we can observe a sub-harmonic mode at 372 Hz for case A at  $\phi = 0.46$ . On comparing the most dominant frequencies for all the three cases at  $\phi = 0.46$ , we observe that the amplitude of case B is relatively smaller than that of case A (20% lower), while there is no significant difference between those of cases A and C. However, we note that the amplitude of the sub-harmonic frequency is significantly smaller for cases B and C on comparison with that of case A. It appears that the higher turbulence intensities cause a larger suppression of the sub-harmonic mode when compared to the most dominant mode at 124 Hz.

To investigate the cause of the reduction in the amplitude of the periodic oscillations at lower equivalence ratios with the inclusion of the flow restrictors, we plot the field of  $\overline{p'q'}(x, y)$ , which is a time-averaged field (averaged over the entire sequence of images for 2.5 seconds), obtained using the instantaneous pressure fluctuations ( $p'(t)$ ) and the instantaneous local heat release rate ( $\dot{q}'(x, y, t)$ ) from the CH\* chemiluminescence images. The boundary conditions of the combustor are approximated as an open-closed duct. Subsequently, we expect a quarter wave mode in the acoustic field during the occurrence of thermoacoustic instability. If we assume the spatially averaged temperature to be 700°C, we obtain the frequency of the

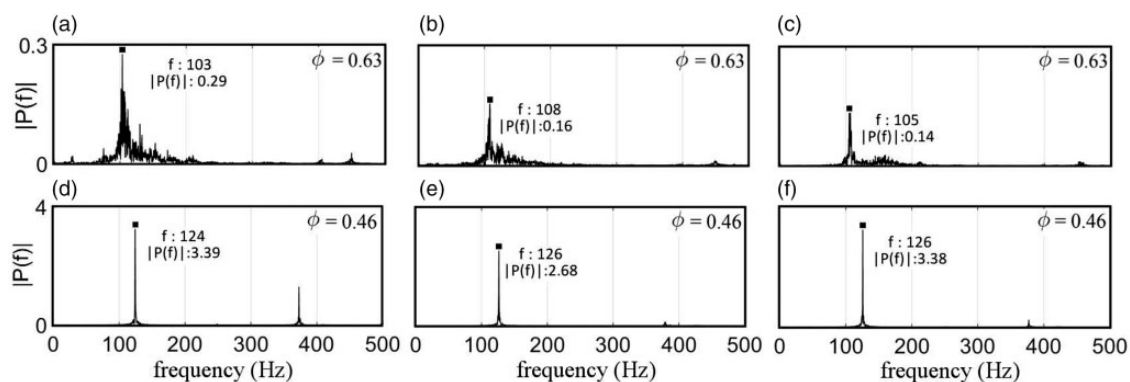


**Figure 5.** Amplitude spectrum of the unsteady pressure fluctuations obtained by fast Fourier Transform (FFT) for case A (a, d), case B (b, e) and case C (c, f) at  $\phi = 0.63$  and  $\phi = 0.46$ .

oscillations as 142 Hz for the fundamental mode. In Figure 6,  $\overline{p'q'}(x, y)$  is shown for the three cases at  $\phi = 0.46$ , where the observed amplitude of the periodic oscillations is maximum. The field of  $\overline{p'q'}(x, y)$  is obtained as the product of the local heat release rate  $\dot{q}'(x, y, t)$  at each pixel of the image and the value of the pressure fluctuation  $p'(t)$  at a particular time instant, which is subsequently averaged over the entire sequence of images of 2.5 s. Lieuwen and Zinn<sup>38</sup> showed that if the length scale of the reaction zone is much less than the acoustic length scale, the variation of the acoustic pressure across the reaction zone is small. Nair<sup>39</sup> had also confirmed this experimentally in the same combustor used for this study. Higher amplitude of the pressure oscillations without the flow restrictors can be associated with a higher strength of the  $\overline{p'q'}(x, y)$  field near the dump plane compared to case B and case C. The higher strength of the  $\overline{p'q'}(x, y)$ , representative of the local acoustic power production drives the thermoacoustic instability for case A, as evident from the previous Figures 3 to 5. Further, we also observe regions of negative  $\overline{p'q'}(x, y)$  near the dump plane for cases B and C.

With the inclusion of the flow restrictors, we can observe in Figure 6 that there is a reduction in the strength of  $\overline{p'q'}(x, y)$  at higher turbulence intensities near the dump plane. Further, for case A, there is a region of positive  $\overline{p'q'}(x, y)$  near the dump plane suggesting spatial coherence in the interaction between the unsteady heat release rate and the acoustic pressure fluctuations. Additionally, we also observe that this region of positive  $\overline{p'q'}(x, y)$  is more dispersed in the cases of higher turbulence intensities, i.e. cases B and C. One could conjecture that the higher turbulence intensity has caused the spatial heat release rate to drift out of phase with the unsteady pressure fluctuations. Furthermore, one could also conjecture that a change in the spatial distribution of the heat release rate results in the reduced amplitude of the pressure oscillations at higher turbulence intensities. These observations could also be linked with changes to the coherent flow structures in the shear layer downstream of the backward facing step. Previous studies by Paschereit et al.<sup>27</sup> and Schadow and Gutmark<sup>25</sup> have shown the presence of coherent flow structures in the flow field during thermoacoustic instability. Further,

they have also reported that the suppression of these coherent flow structures results in the reduction of the amplitude of the pressure oscillations.

A turbulent flame is not a compact source. Further, the interaction between the flame, the hydrodynamics, and the acoustic field leads to complex spatial and temporal phenomena in a thermoacoustic system. Thus, it is critical to investigate the spatiotemporal dynamics during the transition from combustion noise to thermoacoustic instability. It is also important to study the interacting subsystems together ( $p'(t)\dot{q}'(x, y, t)$ ) to study the transition in the turbulent combustor. The instantaneous fields of  $p'(t)\dot{q}'(x, y, t)$  are shown in Figure 7 for different instants at  $\phi = 0.89, 0.82, 0.56$  and  $0.46$ . We observe grainy fields of  $p'(t)\dot{q}'(x, y, t)$  at  $\phi = 0.89$  because of non-similar values of  $p'(t)\dot{q}'(x, y, t)$  at nearby spatial locations. By reducing  $\phi$  to 0.82, regions of similar values of  $p'(t)\dot{q}'(x, y, t)$  emerge near the dump plane during the periodic epochs of intermittency. These regions of coherence or regions of similar values of  $p'(t)\dot{q}'(x, y, t)$  grow bigger in size and magnitude by the reduction of  $\phi$  to 0.56 and subsequently to 0.46, both of which correspond to large amplitude periodic oscillations. Essentially, en route to thermoacoustic instability via intermittency, there is a growth of these coherent regions, which subsequently transfer energy into the acoustic field. Thus, during the transition to thermoacoustic instability, these regions grow slowly with a reduction in the equivalence ratio for the case of swirl-stabilized combustors. Further, these instantaneous fields indicate the likely absence of the helical mode in the combustion dynamics at different equivalence ratios. For all the reported cases in this study, we observe only the axial mode of instability. However, to ascertain the dominant flow structures for different equivalence ratios, a more comprehensive study with simultaneous measurements of the velocity field and chemiluminescence is needed.

Various measures such as spatial variance, spatial skewness, spatial correlation, etc. are adopted to study the transitions in ecological and biological systems.<sup>40</sup> The authors observe that an increase in the spatial variance corresponds with the formation of coherent spatial structures in ecological transitions.

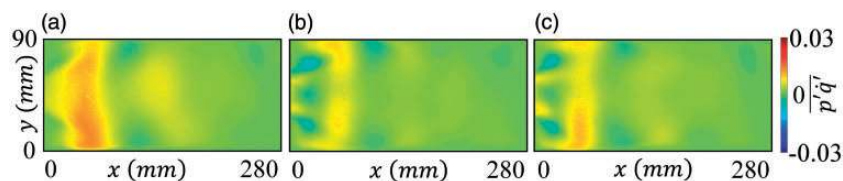


**Figure 6.** Time-averaged field,  $\overline{p'q'}(x, y)$  for case A (a), case B (b) and case C (c) for  $\phi = 0.46$ .

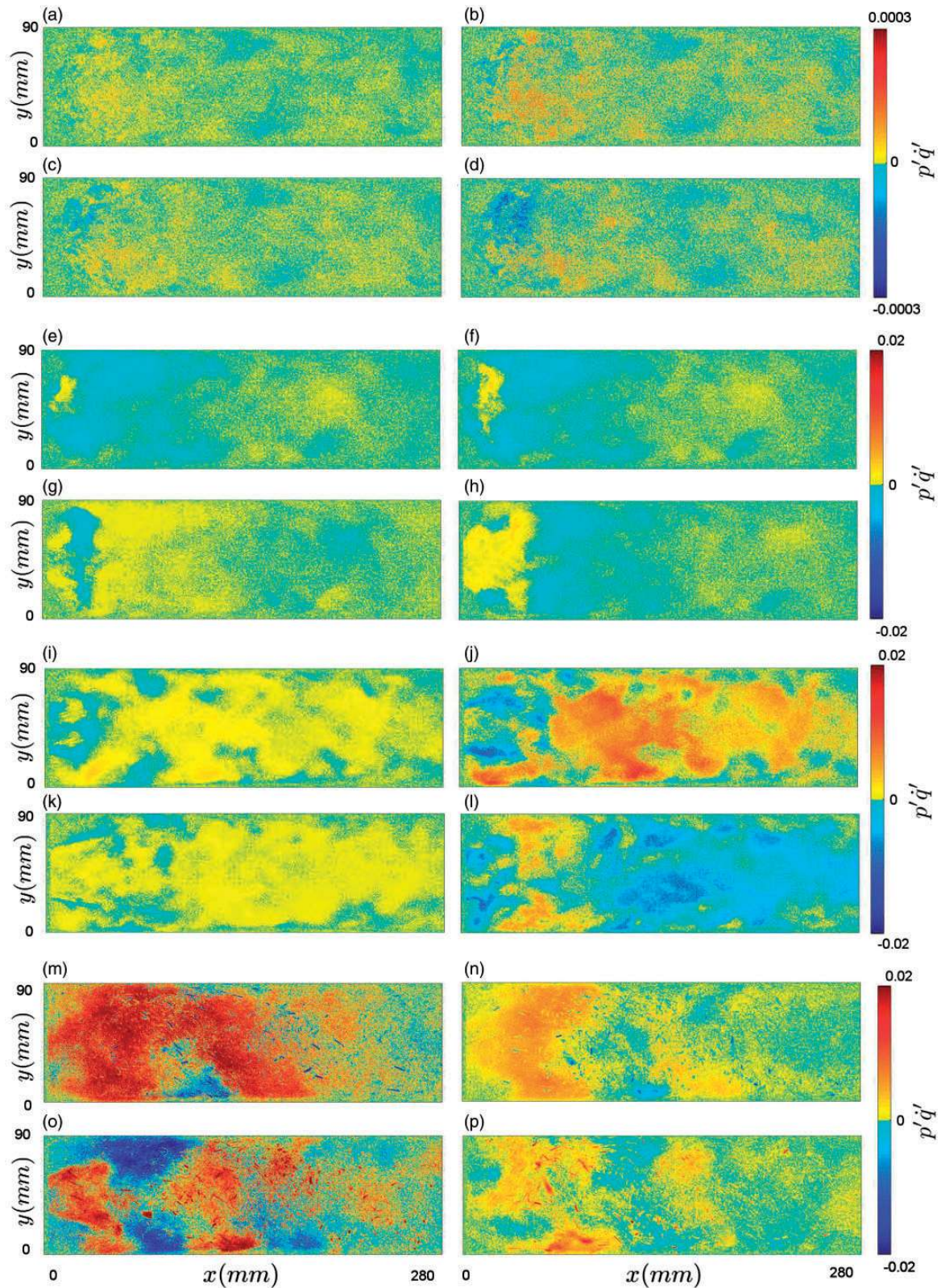


**Figure 7.** Instantaneous fields of  $p'(t)q'(x,y,t)$  for case A at different equivalence ratios  $\phi = 0.89$  (a–d),  $\phi = 0.82$  (e–h),  $\phi = 0.56$  (i–l) and  $\phi = 0.46$  (m–p). m–p correspond to one cycle of acoustic pressure oscillation during the occurrence of thermoacoustic instability. At  $\phi = 0.89$ , the images appear grainy. At  $\phi = 0.82$ , small regions of coherence start to emerge during the periodic epochs of intermittency, although having low magnitude. With further reduction in  $\phi$  to 0.56 and subsequently to 0.46, both of which correspond to large amplitude periodic oscillations, larger and stronger regions of coherence are observed. Note the change in the abscissa for  $\phi = 0.89$ .

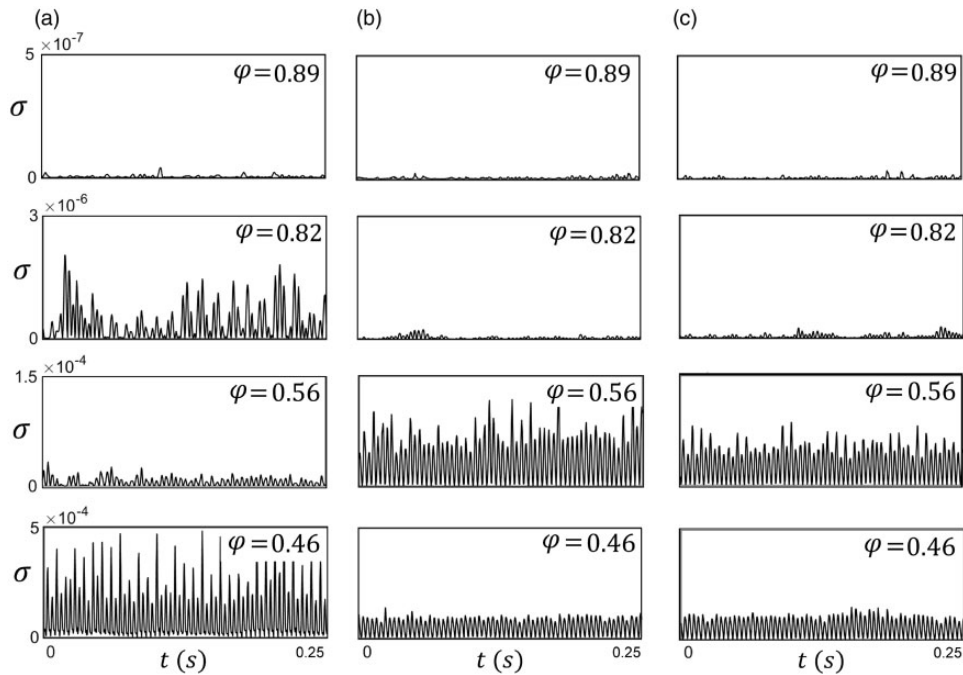
Spatial variance has been used in the past to study the emergence of coherent spatial dynamics in systems undergoing transitions such as ecological systems, biological systems, chemical systems, etc. In our study, we make use of the spatial variance of  $p'(t)\dot{q}'(x, y, t)$  to understand the transition in the turbulent combustor. Spatial variance of  $p'(t)\dot{q}'(x, y, t)$  is calculated as  $\sigma(t) = \sum_x \sum_y (p'(t)\dot{q}'_{xy}(t) - \langle p'(t)\dot{q}'(t) \rangle)^2$  where  $p'(t)\dot{q}'_{xy}(t)$  is the instantaneous local acoustic power production and  $\langle p'(t)\dot{q}'(t) \rangle$  is the instantaneous spatially averaged acoustic power production.

Figure 8 shows the time traces of the spatial variance for different equivalence ratios and for the different levels of turbulence. We remark that even at the higher equivalence ratio  $\phi = 0.82$ , for case A (Figure 8(a)), there is an increase in the spatial variance of the field of  $p'(t)\dot{q}'(x, y, t)$ . This suggests that there is an intermittent emergence of coherent spatial structures in the spatial dynamics at  $\phi = 0.82$ . Thus, one could assume that a transition in the spatial dynamics has already occurred in the combustion dynamics during the state of intermittency where coherent spatial structures start to form amidst incoherent regions. On further reduction of the equivalence ratio to  $\phi = 0.46$ , we also observe large values of spatial variance in Figure 8(a) alternating with the values of low spatial variance in the time trace. This time trace of the spatial variance of  $p'(t)\dot{q}'(x, y, t)$  at  $\phi = 0.46$  illustrates the effect of the impingement of

the large scale vortices, causing simultaneous reaction, resulting in coherence, followed by the dissipation of the coherence in the spatial dynamics of  $p'(t)\dot{q}'(x, y, t)$  during the occurrence of thermoacoustic instability (for one periodic cycle).

Dakos et al.<sup>41</sup> showed that flickering events in the ecological systems between the basins of attraction of the alternative states of the system can occur under noisy conditions which may indicate an impending transition. These flickering events could be identified by the increase in the variance. In our combustor, the increase in the spatial variance at  $\phi = 0.82$  for case A could possibly be due to the occurrence of the intermittent state, which is essentially a state where the system alternates between the two basins of attraction, namely the aperiodic low-amplitude regime and the large amplitude periodic regime under the influence of the turbulent flow fields. Here, the emergence of coherence in the spatial dynamics results in the increase of spatial variance. It is likely that during the state of intermittency, large scale vortices which emerge intermittently in the flow field induce the formation of coherent regions in the field of  $p'(t)\dot{q}'(x, y, t)$ .

Generally, we observe that with a decrease in  $\phi$ , there is an increase in the spatial variance. This shows that there are coherent regions of positive  $p'(t)\dot{q}'(x, y, t)$  which form in the flow field with a decrease in  $\phi$ . However, one should note that these regions do not occupy the entire combustor duct. Coherence in



**Figure 8.** Variation of the spatial variance  $\sigma(t)$  with respect to the equivalence ratio for different cases: case A (a), case B (b) and case C (c). Note that the scale is different for the abscissa for the different equivalence ratios.

$p'(t)\dot{q}'(x, y, t)$  is not observed in the entire reactive flow but in certain locations, mostly near the dump plane. This is the reason why the formation of coherent spatial structures results in the increase of spatial variance as the equivalence ratio is reduced. The transition from combustion noise to thermoacoustic instability via intermittency is thus characterized by the formation of coherent spatial regions in the field of  $p'(t)\dot{q}'(x, y, t)$ . We observe that for the cases B and C (Figure 8(b) and (c)), the spatial variance is smaller than that for case A at  $\phi = 0.46$ . From this, we can infer that the  $p'(t)\dot{q}'(x, y, t)$  in cases B and C is more dispersed relatively to case A in the reactive flow field due to the presence of stronger turbulence. This dispersal results in the reduction of the amplitude of the acoustic pressure oscillations at lower equivalence ratios. However, in Figure 8, at  $\phi = 0.56$ , we observe that the spatial variance of the cases with higher turbulence intensity is more than case A. This corresponds with the advanced onset of large amplitude pressure oscillations for the cases with higher turbulence intensities. Thus, with an increase in the turbulence levels, the advanced onset of thermoacoustic instability is due to the advanced emergence of coherence in the spatial dynamics.

#### 4. Conclusion

In the present experimental study with a swirl-stabilized flame, we investigate the transition regime from combustion noise to thermoacoustic instability by varying the turbulence intensities of the flow field using two different configurations of the flow restrictors. With the reduction in the equivalence ratio, we observed that the onset of large amplitude periodic oscillations is advanced in the case of higher turbulence intensities when compared to case A, which corresponds to lower turbulence intensities. Further, at lower equivalence ratios, we observed a reduction in the  $P_{rms}$  for higher turbulence intensities.

We perform spatial analysis on the field of  $p'(t)\dot{q}'(x, y, t)$  to understand the dynamics in the thermoacoustic system with varying turbulence intensities. We observe that  $\overline{p'\dot{q}'(x, y)}$  decreases near the dump plane with an increase in turbulence intensity at  $\phi = 0.46$ . This results in lower  $P_{rms}$  during thermoacoustic instability for the experiments with the turbulence generator. From the field of  $\overline{p'\dot{q}'(x, y)}$ , we also observe that the higher turbulence intensity causes a dispersion in the patches of positive  $\overline{p'\dot{q}'(x, y)}$ . Using spatial variance to understand the transition from combustion noise to thermoacoustic instability, we find that with a decrease in the equivalence ratio, there is an increase in the spatial coherence of the field of  $p'(t)\dot{q}'(x, y, t)$ . This suggests that the coherence

in the spatial dynamics enhances the interaction or the feedback between the unsteady flame and the acoustic pressure oscillations. For higher turbulence intensities, we observe smaller spatial variance at lower equivalence ratios. This leads us to infer that higher turbulence causes the unsteady pressure fluctuations and most of the local heat release rate fluctuations to drift out of phase with each other. Further, this also leads us to conclude that there is a difference in the distribution of the local heat release rate in space due to the modified flow dynamics causing the dispersal of the coherent spatial structures in the field of  $p'(t)\dot{q}'(x, y, t)$ .

In essence, this study extends the understanding of the spatial dynamics of the flame in the presence of the turbulent flow field on the transition to thermoacoustic instability. Real gas turbine engines work at higher mean velocities with turbulence intensities around 30%. At these conditions, measures such as  $u'/S_l$  and the turbulent Reynolds number are very different from the ones observed in lab scale combustors. However, it is not practical to recreate such conditions at the lab scale. Nevertheless, this study provides a fundamental understanding of the significance of coherent spatial structures at these moderate conditions for limit cycle oscillations. A more comprehensive study is required to truly understand the interaction between the flow field and the flame, which requires simultaneous velocity measurements and flame imaging. Such an investigation on the spatial dynamics could extend the understanding of the interaction between the flame and the turbulent flow field in the presence of the acoustic field.

#### Acknowledgements

We would like to acknowledge Thomas Komarek and Wolfgang Polifke for the combustor design. We acknowledge Tim Lieuwen for suggesting the design of the turbulence generator. We wish to acknowledge Thilagaraj for the drawing of the experimental setup.

#### Declaration of Conflicting Interests

The author(s) disclosed receipt of the following financial support for the research, authorship, and/or publication of this article: The authors would like to acknowledge the European Commission under call FP7-PEOPLE-ITN-2012 within the Marie Curie Initial Training Network Thermo-acoustic and aero-acoustic nonlinearities in green combustors with orifice structures (TANGO) as well as the Gas Turbine Technology Enabling Initiative (GATET), India for financially supporting the study.

#### Funding

The author(s) received no financial support for the research, authorship, and/or publication of this article.

## References

1. Sujith RI, Juniper MP and Schmid PJ. Non-normality and nonlinearity in thermoacoustic instabilities. *Int J Spray Combust Dyn* 2016; 8: 119–146.
2. Lieuwen TC. *Unsteady combustor physics*. UK: Cambridge University Press, 2012.
3. Juniper MP and Sujith RI. Sensitivity and nonlinearity of thermoacoustic oscillations. *Ann Rev Fluid Mech* 2017; 50. <https://doi.org/10.1146/annurev-fluid-122316-045125>
4. Kabiraj L, Saurabh A, Wahi P, et al. Route to chaos for combustion instability in ducted laminar premixed flames. *Chaos* 2012; 22: 023129.
5. Kabiraj L, Sujith RI and Wahi P. Bifurcations of self-excited ducted laminar premixed flames. *J Eng Gas Turbines Power* 2012; 134: 031502.
6. Gotoda H, Nikimoto H, Miyano T, et al. Dynamic properties of combustion instability in a lean premixed gas-turbine combustor. *Chaos* 2011; 21: 013124.
7. Kabiraj L and Sujith R. Nonlinear self-excited thermoacoustic oscillations: intermittency and flame blowout. *J Fluid Mech* 2012; 713: 376–397.
8. Nair V and Sujith RI. Identifying homoclinic orbits in the dynamics of intermittent signals through recurrence quantification. *Chaos* 2013; 23: 033136.
9. Pawar SA, Seshadri A, Unni VR, et al. Thermoacoustic instability as mutual synchronization between the acoustic field of the confinement and turbulent reactive flow. *J Fluid Mech* 2017; 827: 664–693.
10. Unni VR and Sujith RI. Flame dynamics during intermittency in a turbulent combustor. *Proc Combust Inst* 2017; 36: 3791–3798.
11. Kheirkhah S, Geraedts BD, Saini P, et al. Non-stationary local thermoacoustic phase relationships in a gas turbine combustor. *Proc Combust Inst* 2017; 36: 3873–3880.
12. Mondal S, Unni VR and Sujith RI. Onset of thermoacoustic instability in turbulent combustors: an emergence of synchronized periodicity through formation of chimera-like states. *J Fluid Mech* 2017; 811: 659–681.
13. Lieuwen TC. Experimental investigation of limit-cycle oscillations in an unstable gas turbine combustor. *J Propul Power* 2002; 18: 61–67.
14. Nair V and Sujith RI. Multifractality in combustion noise: predicting an impending combustion instability. *J Fluid Mech* 2014; 747: 635–655.
15. Waugh IC and Juniper MP. Triggering in a thermoacoustic system with stochastic noise. *Int J Spray Combust Dyn* 2011; 3: 225–241.
16. Jegadeesan V and Sujith RI. Experimental investigation of noise induced triggering in thermoacoustic systems. *Proc Combust Inst* 2013; 34: 3175–3183.
17. Moeck J, Bothien M, Schimek S, et al. Subcritical thermoacoustic instabilities in a premixed combustor. In: *14th AIAA/CEAS aeroacoustics conference (29th AIAA aeroacoustics conference)*, Vancouver, British Columbia, Canada, 5–7 May 2008, p.2946.
18. Bonciolini G. *Effects of turbulence-induced colored noise on thermoacoustic instabilities in combustion chambers*. PhD Thesis, ETH Zurich, Zurich, Switzerland, 2016.
19. Noiray N and Schuermans B. Deterministic quantities characterizing noise driven hopf bifurcations in gas turbine combustors. *Int J Non Linear Mech* 2013; 50: 152–163.
20. Clavin P, Kim JS and Williams FA. Turbulence-induced noise effects on high-frequency combustion instabilities. *Combust Sci Technol* 1994; 96: 61–84.
21. Kabiraj L, Steinert R, Saurabh A, et al. Coherence resonance in a thermoacoustic system. *Phys Rev E Stat Nonlin Soft Matter Phys* 2015; 92: 042909.
22. Kabiraj L, Saurabh A, Nawroth H, et al. Recurrence analysis of combustion noise. *AIAA J* 2015; 53: 1199–1210.
23. Gopalakrishnan EA and Sujith RI. Effect of external noise on the hysteresis characteristics of a thermoacoustic system. *J Fluid Mech* 2015; 776: 334–353.
24. Gopalakrishnan EA, Tony J, Sreelekha E, et al. Stochastic bifurcations in a prototypical thermoacoustic system. *Phys Rev E* 2016; 94: 022203.
25. Schadow KC and Gutmark E. Combustion instability related to vortex shedding in dump combustors and their passive control. *Prog Energ Combust Sci* 1992; 18: 117–132.
26. Moeck JP, Bourgouin JF, Durox D, et al. Nonlinear interaction between a precessing vortex core and acoustic oscillations in a turbulent swirling flame. *Combust Flame* 2012; 159: 2650–2668.
27. Paschereit CO, Gutmark E and Weisenstein W. Coherent structures in swirling flows and their role in acoustic combustion control. *Phys Fluids* 1999; 11: 2667–2678.
28. Komarek T and Polifke W. Impact of swirl fluctuations on the flame response of a perfectly premixed swirl burner. *J Eng Gas Turbines Power* 2010; 132: 061503.
29. Nair V, Thampi G and Sujith RI. Intermittency route to thermoacoustic instability in turbulent combustors. *J Fluid Mech* 2014; 756: 470–487.
30. PIVview. *PIVTEC GmbH*, [www.pivtec.com](http://www.pivtec.com) (accessed 15 December 2017).
31. Raffel M, Willert CE, Kompenhans J, et al. *Particle image velocimetry: a practical guide*. New York: Springer Science & Business Media, 2007.
32. Wieneke B. Generic a posteriori uncertainty quantification for piv vector fields by correlation statistics. In: *17th international symposium on applications of laser techniques to fluid mechanics*, Lisbon, Portugal, 7–10 July 2014.
33. Marshall A, Venkateswaran P, Noble D, et al. Development and characterization of a variable turbulence generation system. *Exp Fluids* 2011; 51: 611.
34. Videto BD and Santavicca DA. A turbulent flow system for studying turbulent combustion processes. *Combust Sci Technol* 1991; 76: 159–164.
35. Lieuwen TC and Banaszuk A. Background noise effects on combustor stability. *J Propul Power* 2005; 21: 25–31.
36. Horsthemke W and Lefever R. Noise induced transitions. In: Vidal C and Pacault A (eds) *Non-equilibrium dynamics in chemical systems, Proceedings of the International Symposium*, Bordeaux, France, 37 September 1984, pp.150–160. Berlin Heidelberg: Springer Berlin Heidelberg.

37. Aumaître S, Mallick K and Pétrélis F. Noise-induced bifurcations, multiscaling and on-off intermittency. *J Stat Mech* 2007; 7: P07016.
38. Lieuwen TC and Zinn BT. Application of multipole expansions to sound generation from ducted unsteady combustion processes. *J Sound Vib* 2000; 235: 405–414.
39. Nair V. *Role of intermittency in the onset of combustion instability*. PhD Thesis, IIT Madras, Madras, Tamil Nadu, 2014.
40. Kéfi S, Guttal V, Brock WA, et al. Early warning signals of ecological transitions: methods for spatial patterns. *PLoS One* 2014; 9: e92097.
41. Dakos V, van Nes EH and Scheffer M. Flickering as an early warning signal. *Theor Ecol* 2013; 6: 309–317.